2-2-2009

True-Time Delay Steering of Phased Array Radars Using Slow Light

Mark Bashkansky
Naval Research Laboratory

Zachary Dutton
BBN Technologies

Armen Gulian
Chapman University, gulian@chapman.edu

David Walker
Naval Research Laboratory

Fredrik Fatemi
Naval Research Laboratory

See next page for additional authors

Recommended Citation

Bashkansky M., Dutton Z , Gulian A , Walker D., Fatemi F, Steiner, M., True-time delay steering of phased array radars using slow light. Advances in slow and fast light II (Eds.: Shahriar S.M., Hemmer P.R. and Lowell J.R.): *Proceedings of SPIE*, vol. **7226**, 2009, Article # 72260. https://doi.org/10.1117/12.816324

True-Time Delay Steering of Phased Array Radars Using Slow Light

Authors

Mark Bashkansky, Zachary Dutton, Armen Gulian, David Walker, Fredrik Fatemi, and Michael Steiner

Invited Paper

True-Time Delay Steering of Phased Array Radars Using Slow Light

Mark Bashkansky[a], Zachary Dutton[b], Armen Gulian[c,d], David Walker[c], Fredrik Fatemi[e], and Michael Steiner[c]

[a]Code 5613, Naval Research Laboratory, Washington, DC, 20375, USA;
[b]BBN Technologies, Cambridge, MA 02138, USA;
[c]Code 5312, Naval Research Laboratory, Washington, DC, 20375, USA;
[d]SFA, Inc., 20 South Wisner Street, Frederick, MD 21701, USA;
[e]Code 5654, Naval Research Laboratory, Washington, DC, 20375, USA;

ABSTRACT

Application of slow light linear delay to squint-free (true-time delay) steering of phased array radar antennae is discussed. Theoretical analysis is provided on true-time delay radar requirements, including delay precision, amplitude precision, and bandwidth. We also discuss an improvement to the slow light technique based on stimulated Brillouin scattering by using a Faraday rotator mirror that provides temporally stable, linear (with pump power) delay, applicable to practical implementations. Future directions are considered.

Keywords: Antenna arrays, radar, slow light, optical fibers, stimulated Brillouin scattering, Faraday rotator

1. INTRODUCTION: RADAR AND SLOW LIGHT PHYSICS

Phased array radars transmit and receive microwave radiation through an array of antenna elements. Via phase shifting each element by a different and precise amount, a narrow beam is coherently steered in a particular direction without the need for mechanical scanning of the antenna. However, phased arrays run into a fundamental limit in regards to the range resolution. The range resolution of a sensor utilizing pulses of a particular bandwidth B is $R = c/2B$, where c is the speed of light in vacuum. The mentioned limit comes about from an effect known as squinting, which is analogous to chromatic aberration and arises whenever high bandwidth signals are used (see Appendix A for more details). Slow light based on stimulated Brillouin scattering (SBS) is a strong contender for solving this problem, as it produces pure delays in a way that allows fast switching of the delay time. Birefringence in optical fibers induces polarization changes which destabilize the SBS delay, however as described in previous work,[1–4] reflection from a Faraday rotator mirror may be used to cancel the effect of polarization changes. In this work, we review a tolerance analysis of true-time delay[5] and discuss the viability of this SBS-based slow light stabilization scheme for a demonstration of slow light as a true-time delay technique.

For a specific example of squinting, consider a one-dimensional array of antennae at positions x_j, then the appropriate phase shifts to steer a beam into direction θ_0 are $\varphi_0^{(j)} = \omega_0 x_j \sin(\theta_0)/c$, where ω_0 is the (central) RF carrier frequency. (The most commonly used in practice are S-band, $\omega_0/2\pi \sim 3$ GHz, and X-band $\omega_0/2\pi \sim 10$ GHz, so we will concentrate in this article on parameters associated with these bands.) For sufficiently large signal bandwidth B, applying phase shifts $\varphi_0^{(j)}$ leads to squinting. The proper, frequency-dependent shift required for beam steering is $\varphi^{(j)} = \omega x_j \sin(\theta_0)/c$, where $\omega = \omega_0 + \delta$ and $\delta \sim B$ represents a particular frequency component of the signal. By neglecting the frequency dependent part of $\varphi^{(j)}$ (that is, $\delta x_j \sin(\theta_0)/c$), different frequencies get steered into different angles leading to beam loss and distortion.

Examination of $\varphi^{(j)}$ reveals that one needs to apply phase shifts which vary linearly with frequency δ to steer all frequency components coherently into a single direction. If one were to apply varying pulse delays $\tau^{(j)}$ at each element, for example via slow light, one automatically obtains the frequency dependent phase shifts necessary

Further author information: (Send correspondence to A.G.)
A.G.: E-mail: armen.gulian@nrl.navy.mil, Telephone: 1 202 404 1944

Advances in Slow and Fast Light II, edited by Selim M. Shahriar, Philip R. Hemmer, John R. Lowell,
Proc. of SPIE Vol. 7226, 72260A · © 2009 SPIE · CCC code: 0277-786X/09/$18 · doi: 10.1117/12.816324

for wide-band beam steering. This is referred to as true time delay (TTD)[6] in the context of phased array radar. The requirements for implementing TTD depend on a number of factors related to the radar design.

The slow light techniques share the important characteristic that the optical signal delays are quickly and easily controllable by adjustment of an auxiliary pump or control field. This makes many of them applicable to fast and agile beam steering in phased array radars. In order to assess how various techniques (atomic systems, optical fiber techniques, solids, semiconductors, photonic bandgap materials, etc.) could perform in this context, one must consider their performance with regards to providing appropriate delay ranges and precisions, bandwidths, amplitude and phase stability, dynamic range, multiple beam capabilities, and ease of hardware integration into a radar system.

In this article, we first consider the performance of beam steering by phase shifters for a variety of parameters to identify regimes in which TTD are necessary. We then analyze the beam forming with TTD in the presence of delay errors, amplitude errors, and finite bandwidths and identify the necessary characteristics to obtain a certain baseline level of performance. Most of our results are presented for X-band parameters, however, we give corresponding numbers for an S-band system and the results are typically quite easy to generalize to any frequency. Using our analysis, one can assess how suitable various slow light techniques would be for this very promising application of slow light. We then discuss results of a specific implementation of the Faraday rotator mirror-based slow-light scheme for pump power-monitored linear delays. Finally, we consider possible future directions of this work.

2. RADAR REQUIREMENTS FOR TRUE-TIME DELAY

True-time delay eliminates squinting by providing phase shifts that vary linearly with frequency. In particular, the array factor (see Appendix A) becomes

$$A^{(TTD)}(\theta,\omega)=\sum_j a_j \exp\left[i\omega\left(u-u_0\right)x_j/c\right] \tag{1}$$

The actual signal frequency ω (rather than the center frequency ω_0) determines the applied steering phase shift, $\varphi^{(j)}=\omega u_0 x_j/c$. The physical delay applied to achieve this is $\tau_d^{(j)}=\varphi^{(j)}(\omega)/\omega=u_0 x_j/c$. Calculation of the array factor reveals that perfect beam forming is recovered even for large bandwidths. The solid curve in Fig. 1(a) is an example for $N=128$ elements, X-band, with $B=1$ GHz. In a TTD system, a large B can reduce the sidelobe variations, but leaves the main lobe intact.

In order to scan the beam, one must be able to adjust the delays at each element over the required range. Note that only the *relative* delay affects the beam steering, so one would design the system so the element at one end (j =1) would not need any delay adjustment, while the far end element ($j=N$) would have the maximum required adjustable delay range $\tau_d^{(max)}=u_0 L/c$, where $L=N\lambda_0/2$ is the total size of the array. In the extreme limit of 90 degree steering, $u_0=1$ and $\tau_d^{(max)}$ is simply the time for light to propagate a distance L. For an X-band system with $N=128$ elements, and 60 degree steering, $\tau_d^{(max)}=5.5$ ns, while an S-band system with the same number of elements, due to the larger λ_0, would require $\tau_d^{(max)}=18.3$ ns.

2.1. Delay precision

Unintended fluctuations of the individual element delays will degrade the coherent summation needed for beam forming and so one must be able to precisely control them. The dashed and dotted curves in Fig. 1(a) plot array factors where each element is given a random error in delay, with a Gaussian distribution of width $\tau^{(e)}$. One sees a degradation of the main lobe level (MLL). It also elevates the side lobe level and introduces some random fluctuations in the sidelobes, which is an important consideration when performing clutter suppression. Fig. 1(b) plots the MLL loss as a function of $\tau^{(e)}$ for $N=128$. We confirmed that this loss was independent of N in all cases and that 1 dB of loss occurs at $\tau^{(e-crit)}$ =8 ps. This time-scale is related to the time for light propagation across one element which is $\lambda_0/2c=1/2f=50$ ps (though the exact value of the tolerance, $\tau^{(e-crit)}$, depends on our choice of a critical loss, chosen to be 1 dB in this analysis). Note, however, that the *relative* delay control required does depend on N. For example, for $N=128$, $\tau^{(e-crit)}/\tau_d^{(max)}=0.0015$ (or 28 dB dynamic

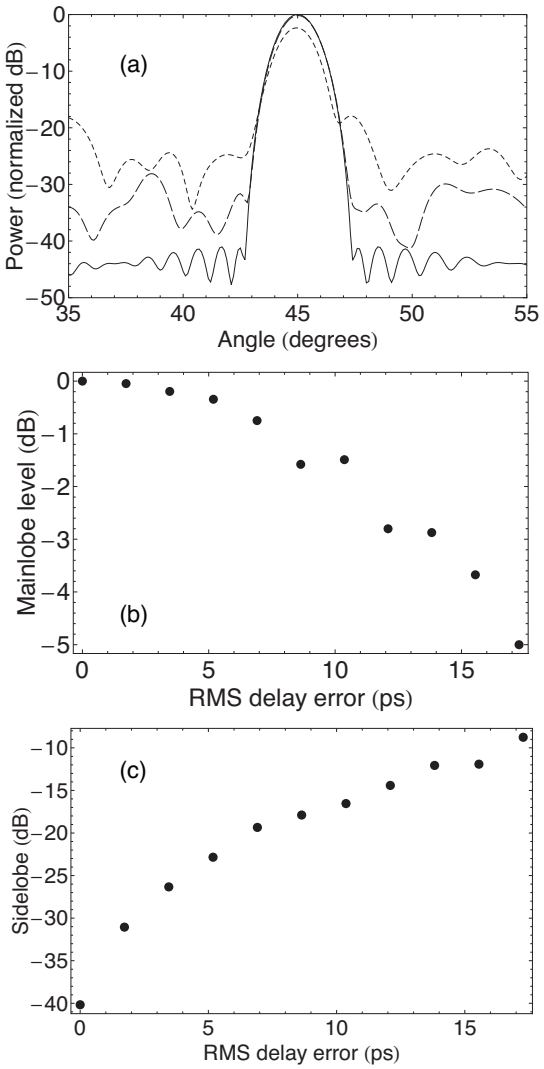

Figure 1. Effect of delay precision in beam forming. $\omega = (2\pi)\,10$ GHz center frequency with $B = (2\pi)\,1$ GHz bandwidth. (a) Array factor $A_B^{(TTD)}(\theta)$ of an $N = 128$ element array with perfect TTD (solid curve) and array factors with RMS fluctuations in the delays of $\tau^{(e)} = 3$ ps (dashed) and $\tau^{(e)} = 11$ ps (dotted) (b) MLL loss at $\theta_0 = 30$ degrees versus delay fluctuation $\tau^{(e)}$. (c) Side lobe level (SLL) at $\theta_0 = 30$ degrees versus delay fluctuation $\tau^{(e)}$.

range) and every factor of two in N will add 3 dB of dynamic range requirement. An S-band radar, would have $\tau^{(e-crit)} = 27$ ps (though a correspondingly larger delay range, so the dynamic range requirement would be the same). For a prototype $N = 4$ array, a relative delay control of 0.05 would suffice.

Note from the beam patterns in Fig. 1(a) that the sidelobe level rises dramatically with delay fluctuations. Fig. 1(c) shows the sidelobe level as a function of the time fluctuation level $\tau^{(e)}$. In particular, at $\tau^{(e-crit)} = 8$ ps, the sidelobe level has gone from the designed (Taylor weighted) level of -40 dB to approximately -21 dB. This has a large effect on clutter suppression and so for many applications the sidelobe requirement will demand more precise delay precision than the main lobe requirement.

In traditional phased array radars, a large amount of calibration and correction is done once the system is constructed, to correct for errors in element spacing, element amplitudes, etc. One can use this same strategy in a TTD system so repeatable, systematic errors in particular delays of particular elements can be corrected in a fielded system. It is only random shot-to-shot fluctuations which must be kept below this critical precision $\tau^{(e-crit)}$.

2.2. Amplitude precision

The other important characteristic is the precision with which the amplitude is preserved by the TTD process. In slow light based on electromagnetically induced transparency (EIT), decoherence will lead to signal attenuation which is related to the delay.[7] Similarly, in fiber-based gain processes, such as stimulated Brillouin scattering, there will be a delay-dependent gain, though there are methods to mitigate this problem.[8] In a TTD radar system, one will need to compensate for these delay-dependent amplitude effects with variable attenuators and/or gain processes (again, as done in calibrating a traditional phased array). However, there will be some residual amplitude errors that will degrade the beam forming. Fig. 2(a) compares the array factor obtained with a perfect TTD with one that has relative amplitude errors of $a^{(e)} = 0.2$. For this calculation, each amplitude a_j is multiplied by a factor $(1 + \alpha)$, where α is chosen from a Gaussian distribution of width $a^{(e)}$. We see that the amplitude errors have no effect on the main lobe, as the elements are all still perfectly phased and have symmetric positive and negative amplitude errors. However, the amplitude errors clearly inhibit the side lobe suppression being performed by the Taylor weighting. Fig. 2(b) plots the largest side-lobe level versus $a^{(e)}$. We lose about 3 dB of suppression for $a^{(e)} = 0.05$ (or 13 dB dynamic range). This is a remarkably weak sensitivity compared to the much more stringent delay precision requirements. In addition to amplitude fluctuations, one can also have independent random phase fluctuations. However, these are mathematically equivalent to the delay fluctuations using the corresponding phase error $\varphi^{(e)} = \omega_0 \tau^{(e)}$. Using this we find the critical phase error level for 1 dB loss is $\varphi^{(e)} = 0.08$.

2.3. Bandwidth

One important consideration in applying slow light methods to beam steering is that, because they rely on the introduction of dispersive features in the index of refraction, they inevitably (by Kramers-Kronig relations) have a finite bandwidth. Generally speaking, the leading order bandwidth effect is due to parabolic frequency dependence of the amplitude gain or loss that leads to pulse broadening.[9] For certain systems, such as EIT in atomic systems,[10] this bandwidth can be quite small (~ 1 MHz) for reasonable pump powers. It is partly for this reason that slow light in semiconducting materials and optical fibers has been pursued recently.[11,12] The bandwidth requirements for radar application are quite clear, since it is the signal bandwidth restriction from squinting (and resulting limitation on range resolution) that first motivated TTD.

A typical 127-bit pulse compression sequence with a 1 ns bit length is shown in Fig. 3(a). These sequences have a time-bandwidth product much greater than unity. After being subject to a finite bandwidth of 1 GHz due to slow light delay mechanism, higher frequency components will be attenuated, resulting in a distorted sequence shown in Fig. 3(b).

Simulations of the beam forming taking into account a finite bandwidth, done by weighting different frequencies according to some attenuation or gain law, show that this has no effect on the array factor other than to attenuate (or apply gain) to the entire pattern. Thus, one can estimate the MLL loss simply by calculating the transmission of the slow light system for a bandwidth of interest.

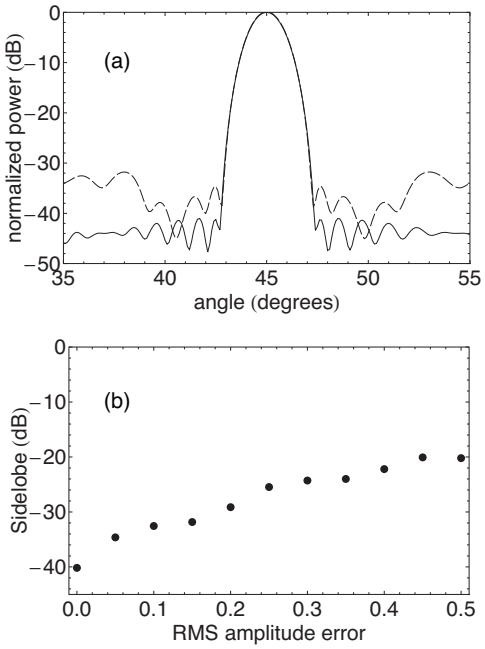

Figure 2. Effect of amplitude fluctuations in beam forming. $\omega = (2\pi)\,10$ GHz center frequency with $B = (2\pi)\,1$ GHz bandwidth. (a) Array factor of an $N = 128$ element array, steering at $\theta_0 = 30$ degrees, with perfect TTD (solid curve) and with amplitude fluctuations $a^{(e)} = 0.2$ (dashed). (b) Maximum SLL versus amplitude fluctuation $a^{(e)}$.

The bandwidth distortion will have a much more direct effect when one considers the signal processing used to obtain range information. Ultimately, the range resolution will be restricted to $R = c/2B$, where B is the bandwidth of the slow light mechanism. We note that, just as known amplitude and phase errors can be calibrated and corrected, known pulse distortion or dispersion effects can sometimes be compensated. However, one will always be limited if a particular frequency component is attenuated significantly with respect to the system noise. This is illustrated in Fig. 3(c) where the solid curve shows auto-correlation between two perfectly transmitted sequences, the dashed and dotted curves show cross-correlation between perfect and filtered sequences with bandwidth of 1 GHz and 0.5 GHz respectively. The dashed curve is the one we wish to use in practice. For these calculations the bit length is one nanosecond and the bandwidth filter applied (B) was a Lorentzian with linewidth of either 1 GHz or 0.5 GHz. This corresponds to the range resolution of approximately $c/2B = 15$ cm (1 GHz) or 30 cm (0.5 GHz). As discussed earlier, besides having a negative impact on the resolution, the finite bandwidth also causes reduction in the signal amplitude.

3. SBS-BASED SLOW LIGHT APPROACH TO PRODUCING TRUE-TIME DELAY

3.1. Theory

In SBS, as it is used for slowing light,[12,13] pump and Stokes beams counterpropagate through a nonlinear medium. When their frequency difference is close to the Brillouin frequency for the medium, their interaction creates an acoustic wave. The pump beam, seeing a refractive index modulation that moves at the speed of sound in the medium, scatters, causing the Stokes beam to be amplified and delayed. The envelope of the acoustic wave is driven by a term proportional to the product of the pump and Stokes fields and their mixing efficiency, k, which is determined by the beam polarizations.

In the absence of birefringence, and when both pump and Stokes are linearly polarized, this mixing efficiency will be 1 when pump and Stokes polarizations are parallel, and 0 when they are orthogonal. As optical fibers typically used for SBS-based slow light have some small amount of random birefringence, the pump polarization will change as it propagates through the fiber, following a random trajectory on the Poincaré sphere. If the

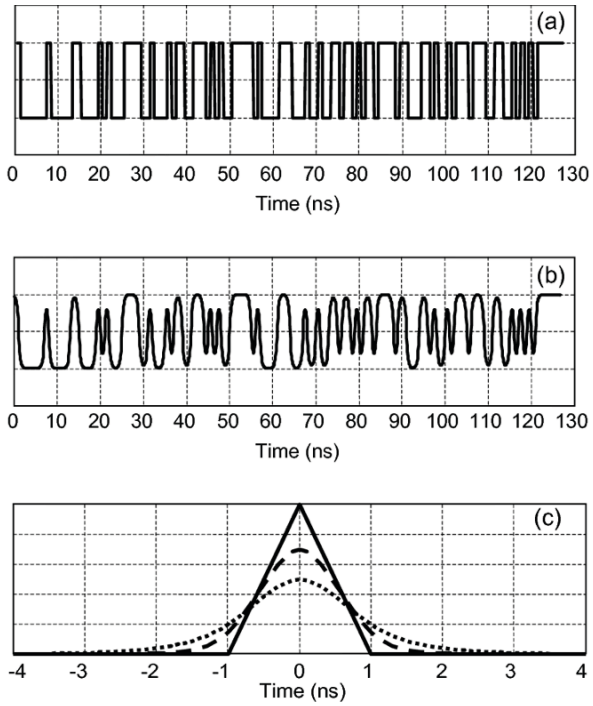

Figure 3. Bandwidth limitations on radar pulse sequences. (a) Typical compression sequence: 7-bit Maximal length sequence with 1 ns bit length, (b) Effect of slow light finite bandwidth of 1 GHz on the sequence (c) Effect of finite bandwidth on the range resolution given by cross-correlation of compression sequences. Solid curve: auto-correlation of perfectly transmitted sequence (a). Dashed curve: cross-correlation of perfect (a) and 1 GHz bandwidth-limited (b) sequences. Dotted curve: cross correlation of perfect (a) and filtered 0.5 GHz bandwidth-limited sequences.

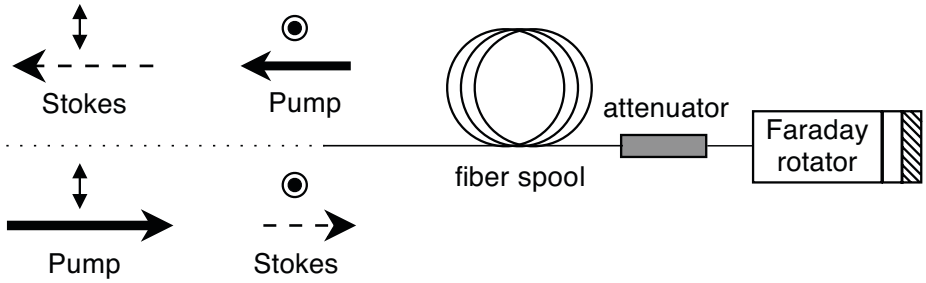

Figure 4. Pump and Stokes are coupled into a spool of fiber from one end with orthogonal polarizations. The Faraday rotator mirror reflects these beams and rotates their polarizations by 90 degrees. As they return, the Stokes now has the correct polarization for maximizing its Brillouin interaction with the counterpropagating pump.

Stokes beam is launched from one end of the fiber, with a polarization ellipse that perfectly overlaps that of the pump beam at that point and with a handedness that matches that of the pump (launched from the opposite end of the fiber), the counterpropagating Stokes beam, seeing the same birefringence as the pump did, will unwind the changes to the pump polarization, so that both the polarization ellipse and handedness of the pump and Stokes continue to coincide at each point along the fiber. (Following van Deventer,[14] we define handedness with respect to the propagation direction of the beam.) Typically, ensuring that the polarization ellipses of the counterpropagating pump and Stokes continue to overlap precisely at one end of the fiber requires that the temperature and physical perturbations of the optical fiber be strictly controlled to avoid the need for repeatedly adjusting beam polarizations.

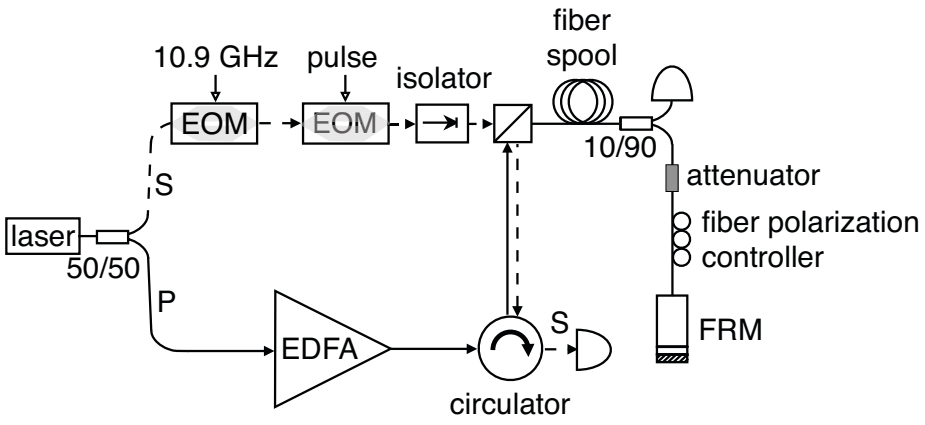

Figure 5. The Faraday rotator mirror configuration for slowing light using SBS, as described in the text. The Stokes beam passes through two Mach-Zehnder electro-optic modulators (EOM) and an isolator before combining with the orthogonally-polarized pump beam at the polarizing beam combiner. It passes through the fiber spool, the 10/90 splitter, an optional 5 dB attenuator and a fiber polarization controller before reaching the Faraday rotator mirror (FRM). On its return, its rotated polarization causes it to emerge from the other port of the beam combiner, where it then passes through the circulator and is detected at the photodetector.

However, if one attaches a Faraday rotator mirror (and an attenuator to eliminate double-pass effects) to one end of the fiber and launches co-propagating, orthogonally-polarized pump and Stokes into the other end (see Fig. 4), one obtains the same overall SBS Stokes gain (a mixing efficiency of $k = 2/3$) as with the same fiber in the conventional scheme when the polarizations have been manually optimized. More specifically, the retroreflected Stokes has its polarization ellipse rotated by the Faraday rotator mirror to exactly overlap that of the pump beam just before the Faraday rotator mirror. The polarization ellipse of the Stokes then follows that of the pump all the way back to the entrance to the fiber, resulting in stable, maximum Stokes gain without need to adjust polarizations. A Faraday rotator mirror was used in a similar way as early as 1999 to measure variations in temperature or strain with optical fibers.[3] Walker, et al.[4] verifed that this scheme allows stabilization of the delays attainable using stimulated Brillouin scattering. In the next section, we review this experiment and discuss its delay precision.

A recently published result[15] shows that a similar, automatically-stabilized mixing efficiency may be obtained for fast light by an entirely different mechanism: Chin and co-authors have shown that as a single optical pulse develops spontaneously generated Stokes, the refractive index modification resulting from the depletion of photons will cause the pulse to advance. And since under high gains, the Stokes is generated with the same sense of rotation as the original beam, this process will then have a mixing efficiency of $k = 1$.

3.2. Experiment

Figure 5 shows the layout for the experimental demonstration. Power from a laser diode (running CW at a wavelength of 1548 nm) is split into two paths. Along the Stokes path, the beam passes through a Mach-Zehnder electro-optic modulator, driven at 10.877 GHz (the Brillouin shift frequency for our optical fiber), creating sidebands at the Stokes and anti-Stokes frequencies. An applied DC voltage suppresses the carrier frequency. A Stanford Research Systems DS345 function generator drives a second modulator which produces a Gaussian pulse train envelope. An isolator prevents feedback into the laser. Along the pump path, light is amplified by an Erbium-doped fiber amplifier (EDFA), passes through a polarization-maintaining circulator, and enters the polarizing beam combiner.

The pump beam and Stokes beam have p- and s-polarizations, respectively. They are combined in a polarizing beam combiner, the output of which is connected to a spool of SMF-28 optical fiber of length L=1.5 km. At the other end of the spool is a Faraday rotator mirror (FRM) which reflects both beams back with their polarizations rotated by 90 degrees. In order to measure the pump power during the experiment, a 10/90 splitter is inserted

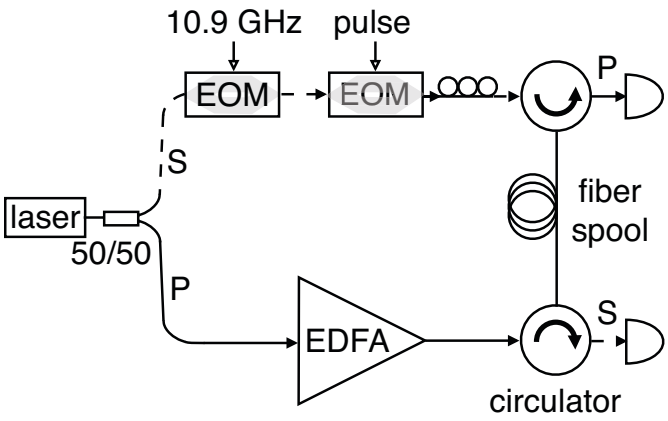

Figure 6. The conventional SBS configuration, as described in the text. Here, two circulators are used to separate and measure the counterpropagating pump and Stokes beams.

between the fiber spool and the Faraday rotator mirror. From the laser diode to the polarizing beam combiner, all the optical fibers in our set-up are polarization-maintaining. Typical powers at the output of the polarizing beam combiner are 50 nanowatts for the Stokes beam and tens of milliwatts for the pump.

A 5 dB attenuator is then inserted between the 10/90 splitter and the Faraday rotator mirror, to allow comparison with the conventional single-pass usage of the same fiber spool. In the presence of the attenuator, the pump beam returning from the FRM is too weak to induce significant Stokes amplification. The Stokes pulse that returns from the Faraday rotator mirror has a polarization ellipse which exactly coincides with that of the counterpropagating pump (see Fig. 4), so the Stokes beam is amplified and delayed as it travels from the FRM back to the polarizing beam combiner. The returning Stokes pulse is p-polarized and is detected at port 3 of the polarization-maintaining circulator with a TTI TIA-500 photodetector which is read with a Tektronix TDS 3052B oscilloscope. Without the attenuator, the reflected pump is sufficiently strong that it will cause the Stokes pulse to also be amplified and delayed as it propagates from the polarizing beam combiner to the Faraday rotator mirror.

As the Stokes pulses are about 200 nanoseconds long (FWHM), they are well within the measured 20 MHz SBS linewidth. We observe negligible pulse broadening for the range of pump powers in this experiment.

For comparison, we also run this experiment in the conventional SBS configuration. The layout is shown in Figure 6. Here, the fiber polarization controller is critical, and the Stokes polarization must be manually adjusted to produce either the best Stokes gain (for pump and Stokes having exactly overlapping polarizations ellipses and the same handedness) or the worst (pump and Stokes having orthogonal polarization ellipses and opposite handedness).

We manually perturb the fiber in the Faraday rotator mirror scheme with the fiber polarization controller and observe no discernible change in the Stokes gain. In contrast, in the conventional SBS scheme, such polarization perturbations cause the gain to vary by a factor of 20 at the same pump power.

By changing the EDFA current, we measure Stokes delay versus pump power in each of these configurations, averaging over 512 shots. The resulting data is shown in Figure 7 . The delay of the pulse is estimated from a fit, assuming that the measured pulse has a Gaussian temporal shape.

The measured delays are in good agreement for the single-pass FRM configuration (represented by open diamonds in the figures) and the conventional SBS configuration where the polarizations have been set for maximum gain (filled triangles).

We believe that the delay noise observed in our experiment is related to the EDFA. The output of the laser diode alone is very stable, both in power and polarization. Adjusting the EDFA current triggers an observable fluctuation in the polarization of the output which slowly decreases in magnitude. The amplifier output interacts

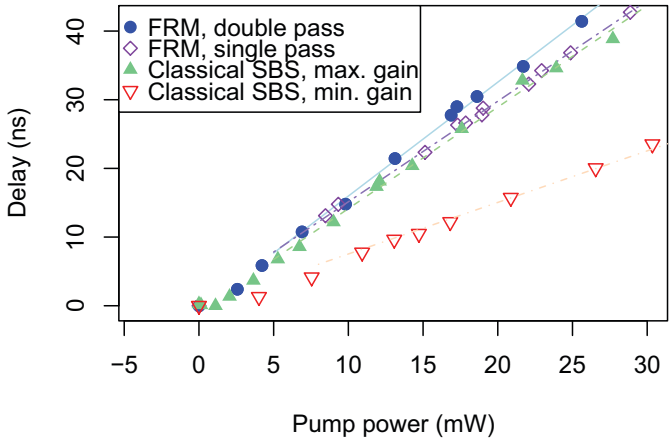

Figure 7. Measured delay versus pump power for various schemes. The circles represent data from the double-pass Faraday rotator mirror scheme. The diamonds show delays from the single-pass FRM configuration. The filled and empty triangles are the delays obtained from the conventional SBS scheme, for polarizations optimized for maximum and minimum delay, respectively.

with the polarization-maintaining circulator, converting the polarization fluctuations into power fluctuations. Eliminating this polarization-to-power conversion noise (with a sufficiently stable EDFA, this should be possible merely by using an external attenuator for amplitude control) should further improve delay precision to that required for a large-N array.

While this experiment was performed within the regular SBS bandwidth, this approach may be adapted to slow light over a much larger bandwidth (though with a corresponding decrease in delay due to the conserved delay-bandwidth product) by broadening the spectrum of the pump beam to accommodate the spectrum of the signal encoded on the Stokes beam.[16,17]

4. FUTURE WORK

Latency (the total time required for the delay element to achieve its relative delay) is an important parameter in a delay element. Fibers made from materials such as chalcogenides rather than silica have larger gain coefficients and therefore require less fiber length (and therefore less time) to achieve the same delay. Storing and retrieving light pulses[18] could allow much shorter latency.

Stimulated Brillouin scattering may also have untapped potential for the creation of high frequency sound waves, in a manner distinct from the thermomodulation approach[19] and compatible with non-conducting materials. Such ultrasonic waves could potentially be used for applications such as superwide-bandwidth all-optical avalanche photon detectors, information transfer with low heat-loads, and non-invasive acoustic imaging.

Noise sources and other possible obstacles to the above objectives include Rayleigh scattering, backscattering from imperfections, and thermally excited sound waves with the resulting Brillouin scattering. Maximizing the efficiency of phonon generation and minimizing the noise sources are critical for photon detection performance.

5. SUMMARY

We have considered how tunable optical time delays using slow light could be exploited to improve the range resolution of phased array radar systems. By considering a basic model for phased array beam steering, we have

calculated the bandwidths at which squinting is introduced into traditional phase shifter systems (using < 1 dB loss of the main lobe as a base requirement). We found that for an X-band system with $N = 128$ elements and ± 60 degree steering capability, squinting attenuates the main lobe for bandwidths $B > 220$ MHz, and that this cut-off scales as $1/N$. True time delay can eliminate this problem, provided one can obtain delay ranges of 5.5 ns for $N = 128$, and delay precision with dynamic range 29 dB. The delay range requirement scales directly with N and inversely with carrier frequency. The sidelobe levels also rise dramatically with delay fluctuations and so must be taken into account in evaluating the slow light mechanisms performance for applications where low sidelobes are required. By contrast, the beam-forming is much less sensitive to amplitude fluctuations of the elements. The main lobe level is not effected by amplitude fluctuations, and amplitude fluctuations of 13 dB end up raising the sidelobe levels 3 dB. Finally, the bandwidth of the slow light mechanism will limit in a direct way the bandwidth of the surviving pulses (especially high time-bandwidth pulse compression sequences) which provide the desired range resolution. In addition, the dynamic range, latency and multiple beam capabilities must also be considered in evaluating the ability of a given slow light mechanism to be used in radar beam steering. As one promising approach to TTD, we have experimentally demonstrated an SBS setup based on a Faraday mirror. Application of slow light for TTD in real phased array radar systems could become possible in the near future.

APPENDIX A. SQUINTING IN PHASE SHIFTER BEAM FORMING

Phase shifters introduce errors for high bandwidth signals (squinting). To quantify this, we consider a one dimensional N =128 element, X-band system, with half-wavelength element spacing: $x_j = j\lambda_0/2$. While radars are usually two-dimensional planar arrays, the squinting effects in each dimension are separable. Thus if squinting results in 1 dB loss in one dimension, then there would be 2 dB loss if one scanned the beam over the same angle range in each dimension (though note that often the steering requirements may be much more severe in one dimension, for example, for a ship-based radar scanning the horizon). We consider scanning angles up to ± 60 degrees. The array factor generated for a beam steered towards angle θ_0, as a function of angle θ and signal frequency ω, is the coherent sum of all the elements,

$$A(\theta, \omega) = \sum_j a_j \exp\left[i\left(\omega u - \omega_0 u_0\right) x_j / c\right] \tag{2}$$

where $u = \sin(\theta)$, $u_0 = \sin(\theta_0)$ and a_j is the element weighting. We will consider here the typical case of Taylor weighting[20] with sidelobe level -40 dB (a uniform weighting gives -15 dB sidelobes). This low sidelobe level is important for clutter suppression algorithms in the signal processing. Note that $\varphi_0^{(j)} = \omega_0 u_0 x_j / c$ represents the phase shift applied to a particular element j. To account for a wideband signal of bandwidth B we consider a uniform integration of the power over the relevant frequencies. This assumes that the signal replica that is used in the radars matched filter[21] is optimized to include the effects of the array, i.e. is the expected received signal from a point target. We then get a beam profile:

$$\left|A_B(\theta)\right|^2 = \frac{1}{B} \int_{\omega_0 - (2\pi)B/2}^{\omega_0 + (2\pi)B/2} \left|A(\theta, \omega)\right|^2 d\omega. \tag{3}$$

The solid curve in Fig. 8(a) shows the beam pattern for steering to 45 degrees for a narrow-band signal ($B = 0$). The 3 dB beam-width is seen to be on the order of 1 degree (generally $\sim 100/N$ degrees) and the sidelobe levels are indeed -40 dB as designed. The dashed and dotted curves then show the results for $B = 300$ MHz and 1 GHz, respectively. As B increases, one sees a severe loss of the MLL and a spreading of the beam. In Fig. 8(b) we plot the MLL versus the relative bandwidth of the signal B/ω_0 for several different steering angles. Because larger phase shifts are needed for larger steering angles, the errors introduced are correspondingly larger. Fig. 8(c) shows the loss versus steering angle for $B = 300$ MHz. Taking an upper limit of 1 dB MLL loss over the entire ± 60 degree scan as a benchmark performance requirement, the squinting problem limits an X-band system to $B < 220$ MHz for this size array. Since the relative bandwidth determines the loss, an S-band system would be limited to $B < 70$ MHz.

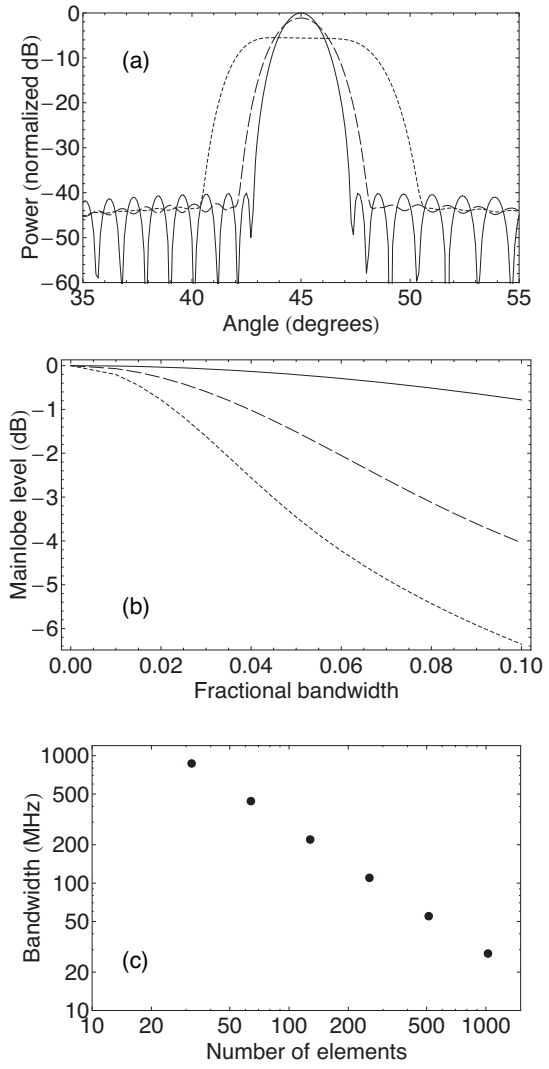

Figure 8. Squinting in phase shifter beam forming. 10 GHz center frequency (X-band) (a) Array factors $A_B(\theta)$ for $B = 0$ (solid curve), 300 MHz (dashed) and 1 GHz (dotted). One clearly sees decrease in the main-lobe level and spreading of the beam. (b) Main-lobe level (MLL) (in dB) versus relative bandwidth, B/ω_0 for steering angles $\theta_0 = 10$ (solid), 30 (dashed), and 60 (dotted) degrees. (c) MLL versus angle θ_0 for B =300 MHz. (d) Bandwidth B at which MLL loss becomes 1 dB at $\theta_0 = 60$ degrees vs. number of elements N.

To obtain better cross-range resolution, arrays use more elements to decrease beam-width $\sim 100/N$. However, doing this makes the main lobe more sensitive to the chromatic dispersion of a particular bandwidth signal B. In Fig. 8(d), we plot the critical point where the MLL loss becomes 1 dB for 60-degree beam pointing versus the number of elements, N. There is clearly a direct $1/N$ scaling in the bandwidth. This plot shows the direct trade-off between cross- and range-resolution present in phased arrays, as the cross-range resolution is determined by the beam width $1/N$ while the range-resolution scales as $1/B$.

ACKNOWLEDGMENTS

This research was supported by the U.S. Office of Naval Research.

REFERENCES

1. Martinelli, M., "A universal compensator for polarization changes induced by birefringence on a retracing beam," Opt. Commun., 72, 341-344 (1989).
2. Laming, R. I. and Payne, D. N., "Electric current sensors employing spun highly birefringent optical fibers," J. of Lightwave Tech., 7, 2084-2094 (1989).
3. Lecœuche, V., Webb, D.J., Pannell, C.N., and Jackson, D.A.,"25 km Brillouin based single-ended distributed fibre sensor for threshold detection of temperature or strain," Opt. Commun., 168, 95-102 (1999).
4. Walker, D. R., Bashkansky, M., Gulian, A., Fatemi, F. K., and Steiner, M. "Stabilizing slow light delay in stimulated Brillouin scattering using a Faraday rotator mirror," J. Opt. Soc. Am. B, 25, C61-C64 (2008).
5. Dutton, Z., Gulian, A., Bashkansky, M., and Steiner, M., [Slow Light: Science and Applications], Ed. Khurgin, J.B., and Tucker, R. S., CRC, (2008).
6. Frigyes, I. "Optically generated true-time delay in phased-array radars," IEEE Trans. Microwave Theory and Techniques, 43, 2378-2386 (1995).
7. Field, J. E., Hahn, K. H., and Harris, S. E., "Observation of electromagnetically induced transparency in collisionally broadened lead vapor," Phys. Rev. Lett., 67, 3062-3065, (1991).
8. Zhu, Z. and Gauthier, D. J., "Nearly transparent SBS slow light in an optical fiber," Opt. Express, 14, 7238-7245, (2006).
9. Boyd, R. W., Gauthier, D. J., Gaeta, A. L., and Willner, A. E., "Maximum time delay achievable on propagation through a slow-light medium," Phys. Rev. A, 71, 023801, (2005).
10. Hau, L. V., Harris, S. E., Dutton, Z., and Behroozi, C. H., "Light speed reduction to 17 metres per second in an ultracold atomic gas," Nature, 397, 594598, (1999).
11. Ku, P. C., Chang-Hasnain, C. J., and Chuang, S. L., "Slow light in semiconductor heterostructures (topical review)," J. Phys. D: Appl. Phys. 40, R93-R107, (2007).
12. Okawachi, Y., Bigelow, M. S., Sharping, J. E., Zhu, Z., Schweinsberg, A., Gauthier, D. J., Boyd, R. W., and Gaeta, A. L., "Tunable all-optical delays via Brillouin slow light in an optical fiber," Phys. Rev. Lett., 94, 153902 (2005).
13. Song, K. Y., Herràez, M. G., and Thévenaz, L., "Gain-assisted pulse advancement using single and double Brillouin gain peaks in optical fibers," Opt. Express, 13, 9758-9765 (2005).
14. van Deventer, M. O., [Fundamentals of bidirectional transfer over a single optical fibre], (Ph.D. thesis, Technische Universiteit Eindhoven, 1994).
15. Chin, S., Herràez, M. G., and Thévenaz, L., "Self-advanced fast light propagation in an optical fiber based on Brillouin scattering," Opt. Express, 16, 12181-12189 (2008).
16. Herràez, M. G., Song, K. Y., and Thèvenaz, L., "Arbitrary-bandwidth Brillouin slow light in optical fibers," Opt. Express, 14 (4), 3951400, (2006).
17. Zhu, Z., Dawes, A. M. C., Gauthier, D.J., Zhang, L., Willner, A. E., "Broadband SBS Slow Light in an Optical Fiber," J. of Lightwave Tech., 25 (1), 201-206, (2007).
18. Zhu, Z., Gauthier, D. J., and Boyd, R. W., "Stored Light in an Optical Fiber via Stimulated Brillouin Scattering," Science, 318, 1748, (2007).
19. Rothenberg, J. E., "Observation of the transient expansion of heated surfaces by picosecond photothermal deflection spectroscopy," Opt. Lett. 13, 713-715 (1988).

20. Trees, H. V., [Optimum Array Processing (Detection, Estimation, and Modulation Theory, Part IV)], John Wiley & Sons, (2002).
21. Skolnik, M., [Radar Handbook], McGraw-Hill, 10.3, (1990).